JOURNAL OF PROPULSION AND POWER
Vol. 20, No. 4, July–August 2004

Autoignited Combustion Testing in a Water-Cooled Scramjet Combustor

Takeshi Kanda,* Nobuo Chinzei,† Kenji Kudo,‡ Atsuo Murakami,‡ and Tetsuo Hiraiwa§
Japan Aerospace Exploration Agency, Miyagi 981-1525, Japan

A water-cooled scramjet combustor was tested to study the effects of pressure, combustor length, fuel-injection style, and wall temperature on autoignited combustion performance. The tests were conducted with an inflow Mach number of 2.5; total pressure of air of 1, 1.5, and 2 MPa; and total temperature of air from 1200 to 2600 K. High-enthalpy air was produced using a vitiation heater. The combustion condition was detected by an increase of temperature in the combustor, which was related to a local combustion condition. When hydrogen fuel was supplied transversely to the combustor wall downstream of the backward-facing step, the autoignited combustion performance degraded with an increase of the airflow pressure under a condition of low total temperature of the vitiated air. The ignition region was around the second explosion limit. The presence of H_2O in the air further retarded ignition under the high-pressure condition. In high-temperature conditions, the combustion performance was improved by the increase of pressure. With the long combustor with a downstream extension, the autoignited combustion limit on the air temperature became lower. A long separation region was presumed to exist downstream of the transverse fuel jet. Under such conditions, the residence time of the mixture increased, and the ability of autoignited combustion could be improved. This effect of the extension of the combustor length decreased with the increase of pressure. Parallel fuel injection from the step base showed low autoignited combustion ability. In the parallel injection, autoignition would initiate at the base of the step, where the pressure was low and the size of the base was small. In the water-cooled combustor, the autoignited combustion limit on the air temperature was higher than that in the uncooled combustor. This fact suggested that the ignition source existed near the wall, for example, in the separation region.

Nomenclature

A	=	cross section of airflow duct
a	=	cross section of fuel injector
D	=	diameter of the fuel injection port
H	=	height of combustor flow path
H_{MID}	=	height of Mach disk in the fuel injected transversely to the wall
M	=	Mach number
$\dot{m}$	=	mass flow rate
P_{ta}	=	total pressure of the vitiated air
P_w	=	wall pressure
q	=	dynamic pressure
T_{ta}	=	total temperature of the vitiated air
V	=	velocity
W	=	width at the exit of the facility nozzle
x	=	distance from the step along flow direction (see Fig. 1)
y	=	vertical distance from the midpoint of the combustor
z	=	spanwise distance from the center plane of the combustor
γ	=	ratio of specific heats
ΔT	=	difference of measured gas temperature after fuel injection from that before injection
ρ	=	density
τ	=	time
ϕ	=	equivalence ratio

Subscripts

ex	=	combustor with extension
f	=	fuel
ig	=	ignition
no_ex	=	combustor with no extension
r	=	residence
∞	=	primary airflow

Received 15 January 2003; revision received 17 September 2003; accepted for publication 25 September 2003.

*Leader, Engine System Team, Combined Propulsion Research Unit, Space Propulsion Research Center, 1 Koganesawa, Kimigaya, Kakuda; kanda.takeshi@jaxa.jp. Senior Member AIAA.

†Director, Space Propulsion Research Center, 1 Koganesawa, Kimigaya, Kakuda; chinzei.nobuo@jaxa.jp. Member AIAA.

‡Senior Researcher, Engine System Team, Combined Propulsion Research Unit, Space Propulsion Research Center. 1 Koganesawa, Kimigaya, Kakuda.

§Senior Researcher, Combustion and Control Team, Combined Propulsion Research Unit, Space Propulsion Research Center, 1 Koganesawa, Kimigaya, Kakuda; hiraiwa.tetsuo@jaxa.jp. Member AIAA.

Introduction

APPLICATION of airbreathing engines to an aerospace plane has been studied in the United States, Russia, Europe, China, Japan, and many countries to create a new transportation system to and form an orbit. An increase of the operating region of an airbreathing engine increases the payload by using oxygen in air. A scramjet engine, which operates in a hypersonic flight condition, will be used in the final stage of the operation of airbreathing engines. The typical operating range of the scramjet is around Mach 7 to 12, and autoignited combustion is attainable because the total temperature of the air is high.

Studies on scramjet combustors and dual-mode combustors have been conducted.[1–3] In most tests, heat-sink combustors, that is, uncooled combustors, have been used because of their low cost.[4–8] However, the heated combustor wall was found to affect autoignited combustion.[7,9] The cooling period of the heated combustor by natural convection becomes long, necessitating a long interval between the tests. Additionally, in a heat-sink combustor the total pressure of the air was restricted as a result of the maximum heat flux in the facility nozzle and the separation limit at the exit. However, the effect of the pressure on combustion is a key issue to design the scramjet combustor and the engine, and the pressure should be a

parameter in the study of the scramjet. On the other hand, in the tests with long, divergent extensions, the autoignited combustion limits were different from that in the combustor with no extension.[8] The study on this effect was, however, difficult in the uncooled test facility because of separation at the exit of the extended duct under the restricted total pressure of the airflow.

A new, water-cooled facility for scramjet combustor tests was constructed. In that facility, the total pressure could be set from 1 to 2 MPa. The effect of the pressure on autoignited combustion was investigated at this facility. The effect of wall temperature on autoignited combustion was examined by comparing the test results from this combustor with those from the heat-sink combustors. The effect of the length of the combustor was also studied with no separation at the combustor exit under the increased total pressure of the airflow. The effect of the fuel-injection method, that is, transverse injection and parallel injection, was also examined for each parameter in the tests.

Experimental Apparatus

Wind-Tunnel and Combustor Model

Figure 1 shows the experimental setup. A scramjet combustor model was directly connected to a blowdown-type wind tunnel. High-enthalpy airflow was created with a hydrogen-air vitiation heater. The total pressure of the air in the reservoir was 1.0, 1.5, or 2 MPa with ± 0.05 MPa fluctuations. The total temperature of the air varied from 1200 to 2600 K. The mole fraction of the unreacted oxygen in the heated air was $21 \pm 1\%$. The mole fraction of the water was, for example, $12 \pm 1\%$ at a 1200 K, $26 \pm 1\%$ at a 2000 K, and $35 \pm 1\%$ at a 2400 K air conditions. Hydrogen was injected into the vitiation heater through 60 elements. Oxygen and air were premixed, and the mixture was injected around each hydrogen injection element. The element was made of a cobalt-base alloy, and the face-plate was made of nickel-base alloy. Figure 2 shows the distributions of oxygen and hydrogen mass fractions, respectively. They were measured at the exit of the supersonic facility nozzle with gas sampling probes and were normalized with the ratios of the supplied oxygen and the hydrogen mass flow rates to the total mass flow rates, respectively. When the value was 1, the mass fraction was equal to that based on the total of supplied gases. The oxygen mass fraction was measured in the noncombusted oxygen-air condition with no hydrogen under an oxygen flow rate of 355 $g \cdot s^{-1}$ and an airflow rate of 2810 $g \cdot s^{-1}$, whereas the hydrogen mass fraction was measured under combustion conditions of $T_{ta} = 1500$ K and $P_{ta} = 1$ MPa. The oxygen and the hydrogen were both uniformly distributed. The vitiated air was accelerated through a rectangular supersonic nozzle.

The Mach number of the nozzle was estimated in two ways. According to the static pressure at the exit of the nozzle and the stagnation pressure in the heater, the Mach number was estimated to be 2.4 under assumptions of isentropic expansion and frozen flow of the ratio of the specific heats of 1.30. Geometrical cross sections were used in the calculation. In the second way, the Mach number upstream of the backward-facing step was estimated to be 2.6 by an empirical equation.[10] These values were around the design Mach number of 2.53. Therefore, the nominal Mach number of this facility was 2.5 in the present testing.

There was an isolator section to eliminate the effect of combustion on the facility nozzle. The isolator had a square section 32 by 147.3 mm. At the end of the isolator, that is, at the entrance of the combustor, there was a backward-facing step of 3.2 mm for flame holding. The step height was based on the criteria of Ref. 11. The x coordinate was along the direction of flow, whereas the y coordinate was perpendicular to the x axis. The z coordinate was perpendicular to the symmetry plane. The origin was at the step (Fig. 1). The cross section of the straight combustor with a constant cross section (CC) was 38.4 by 147.3 mm, with a length of 96 mm. No strut was employed in the present testing.

When the effect of the length of the combustor was investigated, an extension with a divergent angle of 3.4 deg and a length of 240 mm was connected. The cross section of the combustor was 52.8 by 147.3 mm at the exit.

Hydrogen fuel was supplied under sonic condition transversely to the combustor wall 12.8 mm downstream of the backward-facing step or parallel to the wall from the step. In both the transverse fuel-injection and the parallel fuel-injection conditions, there were five fuel injection holes on one side wall and four on the other (Fig. 1, rear view). The pitch between the holes was 32 mm. In the transverse fuel injection, the diameter of each injector hole was 4 mm, except for two holes, the diameter of which was 2.8 mm. This small diameter was for uniformity of the injected fuel concentration. In the parallel injection condition, the diameter of each injector hole was 1 mm, except for two holes, the diameter of which was 0.7 mm. The total temperature of the fuel was about 290 K. The equivalence ratio of fuel was controlled with changing the fuel-injection pressure. The heated air condition became stable 2.5 s after the vitiation heater was started. Fuel injection was then commenced. The period of fuel

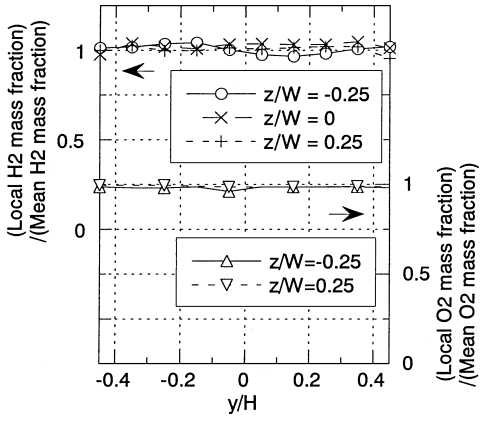

Fig. 2 Distributions of oxygen and hydrogen mass fractions at the exit of the vitiation heater.

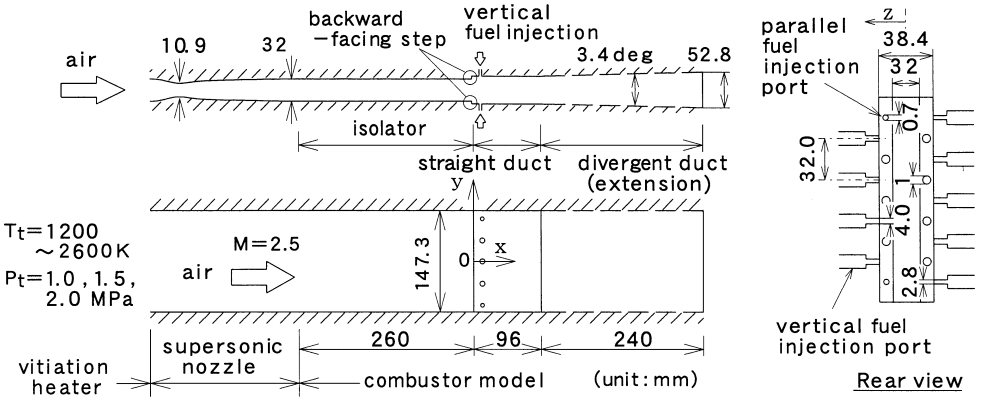

Fig. 1 Schematic diagram of test facility of water-cooled scramjet combustor.

injection was 7 s. The facility and the model were designed for a test duration of 30 s.

The penetration length of fuel injected transversely to the wall is proportional to square root of the ratio of the dynamic pressures of fuel and air as shown[12]:

$$H_{\mathrm{MID}}/D = 1.05[q_f/q_\infty]^{0.5} \tag{1}$$

The dynamic pressure of injected fuel is proportional to the equivalence ratio.

$$\begin{aligned} q_f &= \tfrac{1}{2}\rho_f V_f^2 \\ &= \tfrac{1}{2}(\dot{m}_f/a)V_f \\ &= \tfrac{1}{2}(\phi \cdot \dot{m}_{\mathrm{st}}/a) \cdot M_f\sqrt{\gamma_f R_f T_f} \end{aligned} \tag{2}$$

The ratio of the dynamic pressure of the fuel to that of air is as follows:

$$\begin{aligned} \frac{q_f}{q_\infty} &= \frac{\tfrac{1}{2}(\phi \cdot \dot{m}_{\mathrm{st}}/a)M_f\sqrt{\gamma_f R_f T_f}}{\tfrac{1}{2}(\dot{m}_\infty/A)M_\infty\sqrt{\gamma_\infty R_\infty T_\infty}} \\ &= \phi \cdot \frac{\dot{m}_{\mathrm{st}}}{\dot{m}_\infty} \cdot \frac{A}{a} \cdot \frac{M_f\sqrt{\gamma_f R_f T_f}}{M_\infty\sqrt{\gamma_\infty R_\infty T_\infty}} \end{aligned} \tag{3}$$

Because the mass ratio of air to the stoichiometric fuel is unique, the penetration height of the fuel injected transversely to the wall is proportional to the equivalence ratio. The flow condition in the combustor was similar in spite of the total pressure of the vitiated air under the transverse fuel injection.

The vitiation heater, facility nozzle, isolator, and combustor were cooled with water. The inner wall was made of copper, and the outer shell was constructed of stainless steel. Both were silver soldered. Coolant water, the supply pressure of which was 1.6 MPa, circulated in the channels between the inner and the outer shells. The gas temperature measured through the wall pressure port became approximately steady a second after fuel injection. The wall temperature of the inner copper part was, for example, about 300 K throughout a test at 4 mm from the inner surface and the exit of the CC.

In the heat-sink facility,[4,6] tests of autoignited combustion were conducted to compare its characteristics with those in the water-cooled combustor. Data of the previous tests at the heat-sink facility were also used.[5] The total pressure of the air was restricted at 1 MPa as a result of the maximum heat flux at the nozzle throat and the separation limit at the exit. In the heat-sink facility and the combustor, most of the geometrical configurations were the same as those of the water-cooled facility. The supersonic nozzle diverged on the top and the bottom walls, differing from the water-cooled nozzle represented in Fig. 1. Therefore, the length of the supersonic nozzle was longer than that of the water-cooled facility. The boundary layer of 10 mm in the heat-sink facility[4,7] was estimated to be 1.3 times thicker than that of the water-cooled facility. However, the measured and the estimated Mach numbers at the entrance of the combustor agreed well with each other. It was concluded that there was no significant difference in the flowfield at the entrance of the combustor between the two facilities.

The temperature on the inner surface of the heat-sink combustor was about 600 K at the end of a test, based on measurement by thermocouples.

Measurements

Pressure taps were installed on the line at $y = 0$ mm. The pressure was measured with scanning-type sensors (Scanni valve®) in the 50-ms sampling period and nondimensionalized by the wall pressure at the entrance of the isolator under the condition of no fuel injection. The measurement error of the nondimensional wall pressure was ±0.004.

Thermocouples were inserted into the wall pressure holes in the straight combustor. Their top surface was flush with the inside surface of the combustor. The temperature detected by the thermocouples is designated as measured gas temperature in the present paper. When the increase of the measured gas temperature 1.4 s after the start of fuel injection was more than 100 K, the fuel was presumed to ignite. Gas was pulled out from the wall pressure holes where the thermocouples were inserted, and combustion efficiency was estimated to investigate the relation between the changes of gas compositions and the increase of the measured gas temperature. Sampled gas was analyzed by gas chromatography (Micro-GC CP2002®).

The autoignited combustion conditions were divided into the following five groups, according to the increases of the measured gas temperature:

1) ○, The measured gas temperature increased in all parts (all increase).

2) □, The temperature increased around the step and around the exit of the CC (step and exit).

3) ◇, The temperature increased only around the step (step only).

4) △, The temperature increased only around the exit of the CC (exit only).

5) ×, There was no increase of the temperature in the CC (no increase).

The parentheses contain abbreviations used in the figures. The representative experimental results are shown in Fig. 3. Figure 3a shows the distributions of the increase of the measured gas temperature from that in the no-fuel-injection condition to that in the fuel-injection condition ΔT. Figure 3b shows the wall pressure distributions for the transverse fuel injection with no extension of the

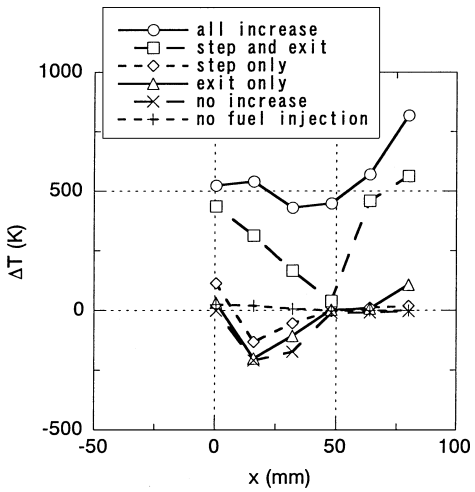

Fig. 3a Increase of the measured gas temperature 1.4 s after the start of fuel injection.

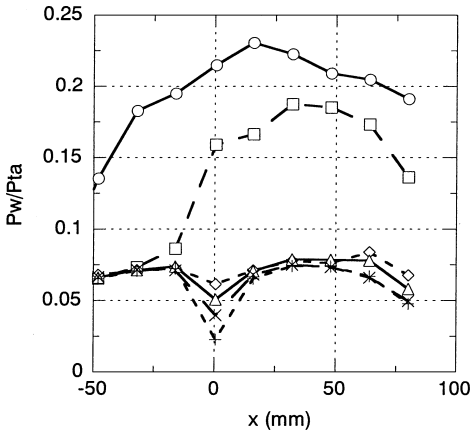

Fig. 3b Wall pressure distributions of five combustion conditions.

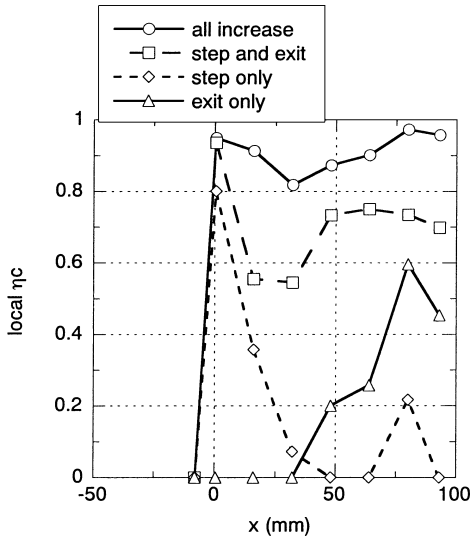

Fig. 3c Local combustion efficiency of four combustion conditions.

combustor. In the ○ condition, ΔT was high throughout the combustor, as was the wall pressure. The pressure began to increase upstream of the combustor. In the □ condition, ΔT dropped at $x = 48$ mm and then increased. The pressure level was high, but there was no increase upstream of the step. In the ◇ condition, ΔT was only at the step. In the △ condition, ΔT at the exit became larger than 100 K. In the × condition, ΔT at the step became smaller than in the ◇ condition, and the subsequent decrease and the recover were observed. The pressure level in the ◇, △, and × conditions was low and approximately the same as that of the no-fuel-injection condition. Figure 3c shows typical distributions of local combustion efficiency of the four conditions. In the ○ condition, the combustion efficiencies were high throughout the combustor. In the □ condition, the efficiencies were high around the step and the exit. In the ◇ condition, the efficiency was high around the step, whereas in the △ condition it was high around the exit. The temperature distribution corresponded to the local combustion distribution. In the present study, measurement of the gas temperature instead of analysis of the gas compositions was adopted to identify the combustion conditions.

In the experiments with transverse fuel injection, autoignited combustion was judged to succeed in the ○ and the □ conditions, and the boundary line of the autoignited combustion was drawn between (○, □) and (◇, △, ×). In the experiments with parallel fuel injection and its comparison with transverse injection, the boundary line was between △ and ×. The other conditions of ○, □, and ◇ were not observed in the parallel fuel injection.

Results and Discussion

Effect of Pressure on Autoignited Combustion

Transverse Fuel Injection

Figure 4a shows results for autoignited combustion with no extension of the combustor. At $P_{ta} = 1$ MPa, the limit of the combustion was at $T_{ta} = 1700$ K and at $\phi = 0.6$. Figures 4b and 4c show the limits of autoignited combustion at $P_{ta} = 1.5$ and 2 MPa, respectively. The limit was at $\phi = 0.4$ at $P_{ta} = 1.5$ MPa, whereas it was at 0.25 at 2 MPa. There were two limits of autoignited combustion: 1) the total temperature limit in the lower temperature condition, which did not depend on the equivalence ratio and varied with the total pressure of the air, and 2) the equivalence ratio limit in the higher temperature condition, which did not depend on total temperature, decreasing as the total pressure increased. The limits are listed in Tables 1 and 2.

At $P_{ta} = 1.5$ or 2 MPa, the limit of total temperature in autoignited combustion of 1) was $T_{ta} = 1800$ K, whereas it was 1700 K at $P_{ta} = 1$ MPa. This meant that autoignited combustion became difficult as the pressure increased in a similar flowfield. The mass flow

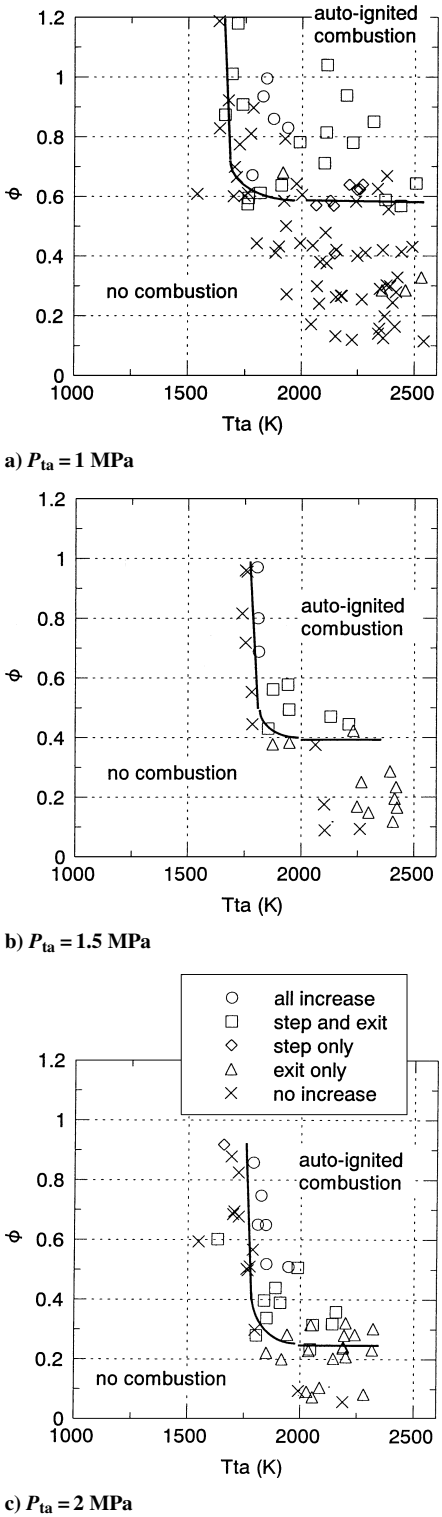

Fig. 4 Autoignited combustion conditions of the water-cooled combustor with transverse injection with no extension.

rate and the dynamic pressure of the air are proportional to the total pressure of the air. The flow rate and the dynamic pressure of the fuel are also proportional to the total pressure of the air at a specified equivalence ratio. There should not be any significant difference in the flow field as a result of the total pressure of the air at the same equivalence ratio, as can be seen in Eqs. (1) and (3). The observed feature suggested that the difference was caused by the effect of pressure level on the chemical reaction.

In such a fuel-injection condition, the injected fuel interacted with the airflow behind the step, and a separation region was

Table 1 Autoignited combustion limit of T_{ta} with transverse fuel injection (unit, K)

P_{ta}	1 MPa	1.5 MPa	2 MPa
No extension	1700	1800	1800
Extension	1300	1500	1600

Table 2 Autoignited combustion limit of ϕ with transverse fuel injection

P_{ta}	1 MPa	1.5 MPa	2 MPa
No extension	0.60	0.40	0.25
Extension	0.50	0.30	0.20

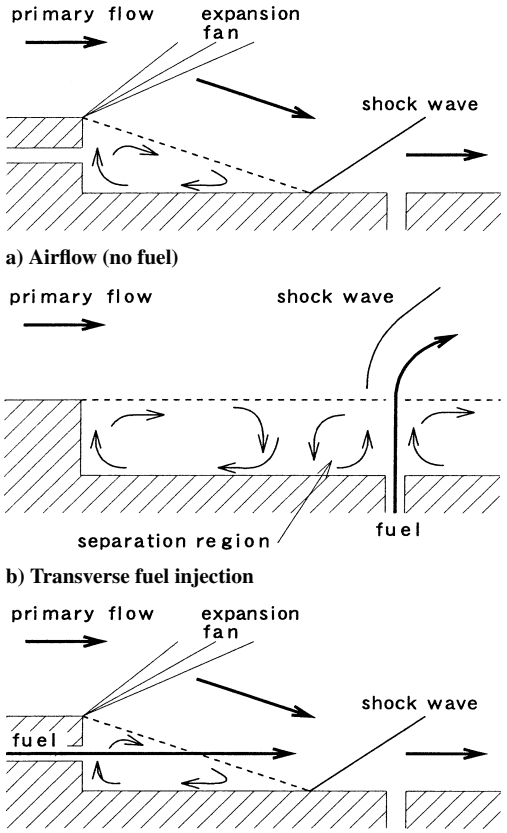

Fig. 5 Schematic diagram of fuel–airflow interaction.

created between the step and the injected fuel.[9,13] Figure 5b shows a schematic diagram of the interaction between the airflow and the fuel jet. The pressure in the region was approximately the same as that of the primary flow upstream of the step before ignition and combustion. In this region, the temperature recovered, and the residence time of fuel was long. Autoignition was presumed to start here. The temperature of the mixture of the fuel and the air was lower than the total temperature of the air because of lower temperature of the fuel and heat transfer to the wall. For example, the temperature of the mixture becomes 1200 K at the stoichiometric condition under the total temperature of the air of 1500 K and the adiabatic wall boundary condition. The temperature and the pressure conditions in the region were around the second explosion limit of hydrogen air. The limit is in a temperature range of 1100 to 1200 K and a pressure rang of 100 to 1000 kPa (Ref. 14). The presence of H_2O in the vitiated air further retarded the ignition because of its large third body efficiency in the reaction of $H + O_2 + H_2O \rightarrow HO_2 + H_2O$ at temperatures less than about 1000 K (Refs. 15 and 16). In the low temperature condition, the presence of H_2O increased the ignition time significantly with the increase of pressure. The effect had been

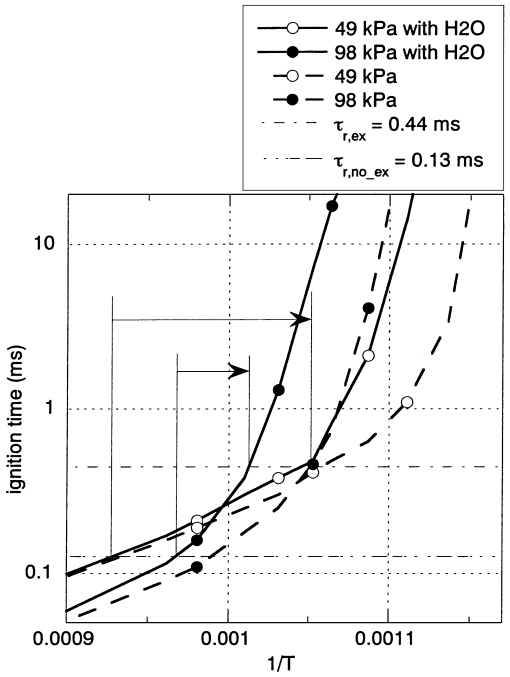

Fig. 6 Calculated ignition times with and without water: $\phi = 1$, $P = 49$ kPa, and 98 kPa correspond to $P_{ta} = 1$ and 2 MPa, respectively. Estimated residence times of the combustor with no extension and that with extension are also plotted.

reported in the range of pressure from 20 to 200 kPa (Refs. 15 and 16).

Figure 6 shows ignition times calculated with the kinetics of Rogers and Schexnayder,[15] which consists 60 reactions and 20 species, using LSENS[17] under the stoichiometric condition. Under the autoignited combustion condition, the equivalence ratio was 1 to 4 downstream of the step, according to the measured compositions of the gas pulled from the wall pressure holes. Ignition time was defined as 5% increase of equilibrium temperature of the reacted gas as was in Ref. 15. In the vitiated air condition, initial mole fractions of oxygen, water, hydrogen, nitrogen, and argon were 0.148, 0.067, 0.295, 0.484, and 0.006, respectively. In the air condition, which had no water vapor in the initial condition, the fractions were 0.148, 0, 0.295, 0.551, and 0.006, respectively. The pressure conditions were 49.2 and 98.4 kPa, which corresponded to the present test conditions of $P_{ta} = 1$ and 2 MPa, respectively. As can be seen, the ignition time was longer in the high pressure condition in the air condition. The time further retarded with presence of H_2O in the vitiated air, as explained in Refs. 15 and 16. The temperature range in the calculation was lower than the total temperature of the vitiated air in Table 1. The temperature of the mixture becomes lower as a result of lower temperature of fuel, and the temperature decreases about 300 K lower than the temperature of the air under the stoichiometric and adiabatic wall conditions. The range of temperature in the calculation would be in actual range of temperature of the mixture.

The second feature was 2) the decrease of the limit of the equivalence ratio with the increase of the total pressure. This appeared in the higher temperature region, so that the mixture condition was beyond the second explosion limit. In such a hot condition, radicals in the vitiated air promoted ignition, and the autoignition time decreased.[14,15] At such a low equivalence ratio, the fuel jet did not interact with the airflow, and there was no separation region between the fuel jet and the step. However, the combustion time also became shorter with an increase of pressure.[14,15] As the total pressure of the air increased, the pressure around the fuel injector became higher. A smaller separation region around the fuel jet with a smaller equivalence ratio, a smaller increase of the local pressure, and a shorter residence time would be sufficient for autoignited combustion under higher pressure condition.

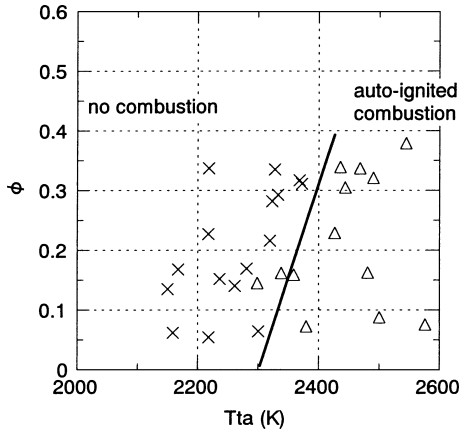

a) $P_{ta} = 1$ MPa

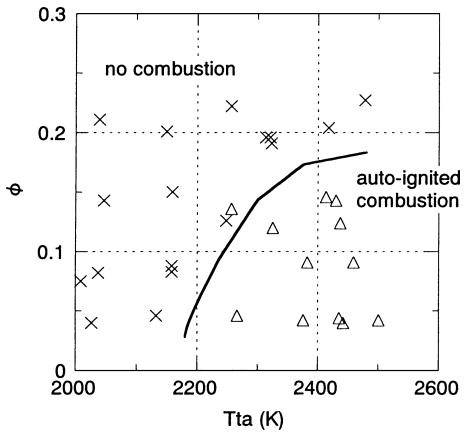

b) $P_{ta} = 1.5$ MPa

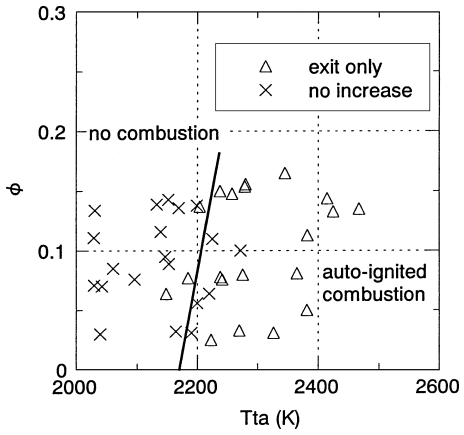

c) $P_{ta} = 2$ MPa

Fig. 7 Autoignited combustion conditions of the water-cooled combustor with parallel injection with no extension.

Parallel Fuel Injection

Figures 7a–7c show the autoignited combustion conditions with the parallel fuel injection. Because the parallel fuel-injection holes were small, the equivalence ratio was up to 0.4 in this facility. In the tests with parallel fuel injection, only the condition of △ and × were observed. The combustion performance of the parallel fuel injection was significantly lower than that of the transverse fuel injection.

As the equivalence ratio increased, autoignited combustion was not easily attained. As the total temperature of the air increased, the limit of the equivalence ratio widened. Comparing Figs. 7a–7c, it shows that the temperature limit spread with the increase of the pressure level.

In parallel injection, the fuel was injected from the step base. The region was small and the pressure in the region was significantly lower than that of the primary flow. Figure 5c shows a schematic diagram of the flowfield. The mixture condition was beyond the second explosion limit. When the total temperature of the air was high, autoignition could occur in the base region. As the equivalence ratio became large, the temperature of the mixture became too low for autoignition. As the total temperature of the air became low, the temperature of the mixture was also too low to autoignite. In parallel fuel injection, the increase of the equivalence ratio would be difficult under the autoignited combustion condition.

The reaction time was estimated to be about 0.5 ms at the flow condition in the preset combustor, that is, a static pressure of about 50 kPa and a static temperature of about 1000 K. There, the reaction time was defined as the time of increase from 5 to 100% of the equilibrium temperature.[15] The core flow velocity of the air was about 1000 $m \cdot s^{-1}$, and the reaction length was about 0.5 m. This was of the same order as the length downstream of the step in the straight combustor, and the reaction probably increased the temperature around the exit of the combustor. The reaction time increases with a decrease of pressure. The low pressure in the base region was unfavorable for reaction of the mixture. The ignition might progress in the base region, but the reaction hardly progresses in that region. Furthermore, the size of the region was too small to remain during the reaction time. The reaction was able to progress out of the base region only under the recovered static pressure condition.

In transverse fuel injection, as well as in parallel injection, when the equivalence ratio was below 0.4, there was no △ condition at $P_{ta} = 1$ MPa, as shown in Fig. 4a. At $P_{ta} = 1.5$ and 2 MPa, autoignited combustion with the △ condition was attained in the region of high temperature and relatively high equivalence ratio region, as shown in Figs. 4b and 4c. The boundary of autoignited combustion showed a feature different from that of parallel fuel injection, even at the same, small equivalence ratio. Below an equivalence ratio of 0.5, the interaction between the fuel jet and the airflow behind the step was weak, and the separation region just upstream of the fuel jet would be the autoignition region.[9] The penetration of the fuel jet was small at a small equivalence ratio as seen in Eqs. (1) and (3). Thus, autoignition at the small equivalence ratio was not easily attained with transverse fuel injection. The ignition regions were quite different between transverse injection and parallel injection, even at the same, small equivalence ratio.

Effect of Length of Combustor on Autoignited Combustion

Transverse Fuel Injection

Figure 8 shows the wall pressure distributions of the autoignited combustion condition (□), the no-temperature-increase condition (×), and the no-fuel-injection condition at $P_{ta} = 1$ MPa with the combustor extension. In the no-fuel-injection condition, there was no pressure increase in the extension except around the exit. Thus, there was no effect of separation on autoignited combustion in the straight combustor section even at $P_{ta} = 1$ MPa. Figure 9 shows the

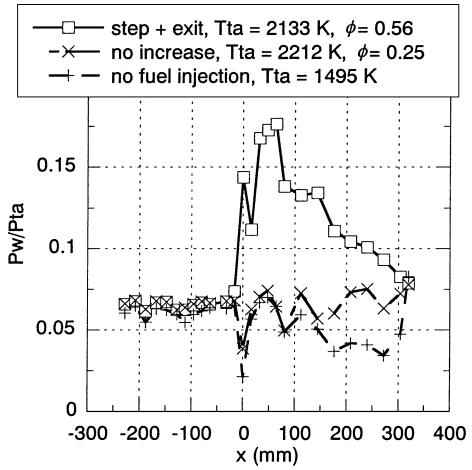

Fig. 8 Pressure distributions with extension at $P_{ta} = 1$ MPa. Fuel was injected transversely.

autoignited combustion limits in the combustor with the extension and in that with no extension at $P_{ta} = 1.5$ MPa. The autoignited combustion limit in the combustor with the extension moved 300 K lower in temperature and 0.1 lower in equivalence ratio than that with no extension. When the total pressure was 2 MPa, the limit moved 200 K lower and 0.05 lower in equivalence ratio. The limit at the total pressure of 1 MPa moved 400 K lower and 0.15 lower in equivalence ratio than the limit in the combustor with no extension. The extension of the combustor widened the autoignited combustion limit to a lower temperature region and a lower equivalence ratio. The results are shown in Tables 1 and 2.

The other conditions were unchanged, so that the attachment of the extension to the straight combustor was presumed to increase the residence time of the mixture in the combustor and to allow longer ignition time. This suggested the existence of a long separation region downstream of the injector, continuing to the extension. The flame in the extension would travel upstream in the separation region to the step.

When the total pressure of the air was high at 1.5 or 2 MPa, the temperature limit of autoignited combustion became high, comparing to the limit at 1 MPa. This feature was the same as that observed in the combustor with no extension. The ignition condition was also around the second explosion limit. The existence of water vapor in the vitiated air further retarded ignition. When the total pressure of the air was high, the effect of the extension on the temperature limit of autoignited combustion was small. The ignition time of the vitiated air increased rapidly with a decrease of temperature at high pressure around 100 to 200 kPa, and the ignition time became longer than the time at lower pressure.[15,16]

Here, the residence time in the separation region is estimated with the sound velocity and the length from the step to the exit of the combustor. Under the stoichiometric condition, mean molecular weight of the mixture of the fuel and the air is 19.7 at the vitiated air temperature of 1600 K. The residence time becomes 0.13 ms in the combustor with no extension and 0.44 ms in the combustor with the extension. In Fig. 6, residence time of fuel in the combustor with no extension τ_{r,no_ex} and that with the extension $\tau_{r,ex}$ are indicated. By attachment of the extension, a longer ignition time is possible because of longer residence time, and ignition is possible at a lower temperature of the mixture. Under the low pressure condition, the temperature limit of autoignited combustion changes from 1080 to 950 K by attachment of the extension. Under the high pressure condition, it changes from 1030 to 990 K. In the extended combustor, higher temperature is necessary for ignition under a higher pressure condition, and lower temperature is allowed for ignition under a lower pressure condition around the present calculation conditions of temperature, pressure, and residence time. The preceding mechanism on the temperature limit of autoignited combustion would be a reason of the difference on the temperature limit caused by attachment of the extension in the experiment.

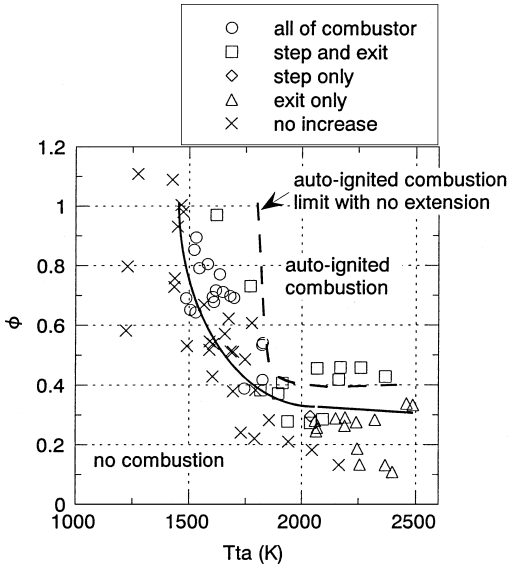

Fig. 9 Autoignited combustion conditions of water-cooled combustor with transverse injection with extension at $P_{ta} = 1.5$ MPa.

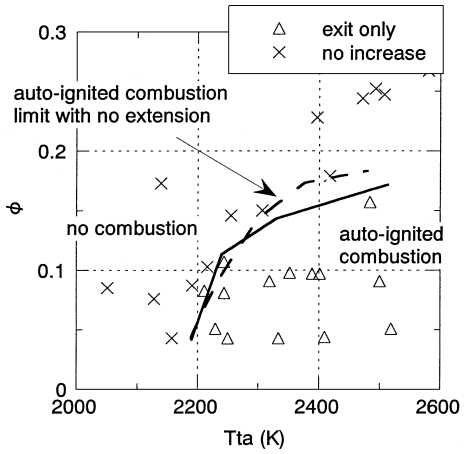

Fig. 10 Autoignited combustion conditions of water-cooled combustor with parallel injection with extension at $P_{ta} = 1.5$ MPa.

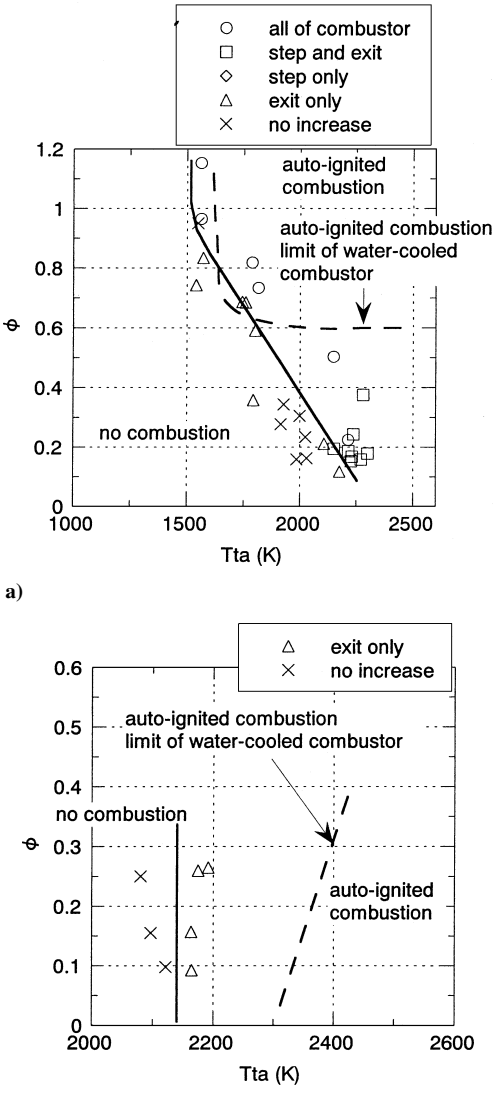

Fig. 11 Autoignited combustion conditions of heat-sink type combustor with no extension, with $P_{ta} = 1$ MPa: a) transverse injection and b) parallel injection.

Parallel Fuel Injection

Figure 10 shows the autoignited combustion boundary with parallel fuel injection at $P_{ta} = 1.5$ MPa. There was no significant difference in the combustion limit as a result of extension of the combustor at this pressure, as well as at $P_{ta} = 1$ MPa and $P_{ta} = 2$ MPa. This was because the ignition region was restricted at the base of the step both with the extension and without the extension.

Effect of Wall Temperature on Autoignited Combustion

Figures 11a and 11b show the autoignited combustion limits in the heat-sink type combustor and in the water-cooled one. There was no extension to the combustor. The total pressure of the air was 1 MPa.

In the heat-sink-type combustor with transverse fuel injection, the equivalence ratio limit decreased with the increase of total temperature. In the water-cooled combustor, the limit of the equivalence ratio did not change greatly above 1800 K. The autoignited combustion limit of the water-cooled combustor showed a narrower range. This implied that the wall temperature had a significant effect on autoignited combustion and that the ignition region was near the wall, as was reported in Ref. 9. The ignition process is significantly affected by temperature. As described in the preceding section, the source of autoignition was in the separation region between the fuel jet and the step. In the heat-sink combustor, the temperature of the mixture in the separation region would be higher than in the water-cooled combustor because of smaller heat loss to the wall.

In the heat-sink combustor with parallel fuel injection, the autoignited combustion limit of the temperature was lower than that of the water-cooled combustor. No limit of the equivalence ratio was observed. This fact also supports the suppositions that the ignition region was near the wall and that the ignition process would still continue even outside the base region.

Conclusions

Autoignited combustion of a water-cooled scramjet combustor was studied experimentally at air total pressures of 1, 1.5, and 2 MPa and at air total temperatures from 1200 to 2600 K. Hydrogen fuel was injected transversely or parallel to the engine wall. Effects of pressure, length of combustor, fuel-injection style, and wall temperature on the autoignited combustion ability were examined. From the tests, the following points were clarified:

1) Autoignited combustion with transverse fuel injection was degraded with the increase of airflow pressure under lower air-temperature condition. The ignition region was around the second explosion limit. The presence of water in the vitiated air further retarded ignition. Such ignition conditions would exist in the separation region around the fuel jet.

2) Under higher air-temperature conditions, the region of autoignited combustion widened with an increase of pressure.

3) The extended combustor showed a wider autoignited combustion region. A long separation region was presumed to exist downstream of the transverse fuel jet.

4) Parallel fuel injection from the step base showed low autoignited combustion ability. Autoignition commenced at the base, where the pressure was low and the size was small.

5) The water-cooled combustor showed a smaller autoignited combustion region than that of the uncooled combustor. This suggested that autoignition was attained near the wall, for example, in the separation region, where the wall condition significantly affected the mixture.

Acknowledgment

The authors thank Tohru Mitani of Japan Aerospace Exploration Agency for advice on ignition.

References

[1]Billig, F. S., "Research on Supersonic Combustion," *Journal of Propulsion and Power*, Vol. 9, No. 4, 1993, pp. 499–514.

[2]Rogers, R. C., Capriotti, D. P., and Guy, R. W., "Experimental Supersonic Combustion Research at NASA Langley," AIAA Paper 98-2506, June 1998.

[3]Cockrell, C. E., Jr., Auslender, A. H., Guy, R. W., McClinton, C. R., and Welch, S. S., "Technology Roadmap for Dual-Mode Scramjet Propulsion to Support Space-Access Vision Vehicle Development," AIAA Paper 2002-5188, Sept. 2002.

[4]Chinzei, N., Komuro, T., Kudo, K., Murakami, A., Tani, K., Masuya, G., and Wakamatsu, Y., "Effects of Injector Geometry on Scramjet Combustor Performance," *Journal of Propulsion and Power*, Vol. 9, No. 1, 1993, pp. 146–152.

[5]Sato, Y., Sayama, M., Masuya, G., Komuro, T., Kudo, K., Murakami, A., Tani, K., and Chinzei, N., "Experimental Study on Autoignition in a Scramjet Combustor," *Journal of Propulsion and Power*, Vol. 7, No. 5, 1991, pp. 657, 658.

[6]Komuro, T., Kudo, K., Masuya, G., Chinzei, N., Murakami, A., and Tani, K., "Experiment on a Rectangular Cross Section Scramjet Combustor," National Aerospace Lab., NAL TR-1068, Tokyo, Japan, June 1990 (in Japanese).

[7]Kudo, K., Komuro, T., Masuya, G., Murakami, A., Tani, K., Wakamatsu, Y., Kanda, T., and Chinzei, N., "An Experiment on Ignition in a Rectangular Cross Section Scramjet Combustor," National Aerospace Lab., NAL TR-1080, Tokyo, Japan, Sept. 1990 (in Japanese).

[8]Kudo, K., Masuya, G., Komuro, T., Murakami, A., and Chinzei, N., "Autoignition and Flameholding in a Cylindrical Scramjet Combustor," National Aerospace Lab., NAL TR-1067, Tokyo, Japan, May 1990 (in Japanese).

[9]Huber, P. W., Schexnayder, C. J., Jr., and McClinton, C. R., "Criteria for Self-Ignition of Supersonic Hydrogen-Air Mixtures," NASA TP 1459, May 1979.

[10]Lamb, J. P., and Oberkampf, W. L., "Review and Development of Base Pressure and Base Heating Correlations in Supersonic Flow," *Journal of Spacecraft and Rockets*, Vol. 32, No. 1, 1995, pp. 8–23.

[11]Diskin, G. S., and Northam, B., "Effects of Scale on Supersonic Combustor Performance," AIAA Paper 87-2164, June 1987.

[12]Cohen, L. S., Coulter, L. J., and Egan, W. J., Jr., "Penetration and Mixing of Multiple Gas Jets Subjected to a Cross Flow," *AIAA Journal*, Vol. 9, No. 4, 1971, pp. 718–724.

[13]Tomioka, S., Hiraiwa, T., Mitani, T., Zamma, Y., Shiba, H., and Masuya, G., "Auto Ignition in a Supersonic Combustor with Perpendicular Injection Behind Backward-Facing Step," AIAA Paper 97-2889, July 1997.

[14]Mitani, T., Hiraiwa, T., Sato, S., Tomioka, S., Kanda, T., and Tani, K., "Comparison of Scramjet Engine Performance in Mach 6 Vitiated and Storage-Heated Air," *Journal of Propulsion and Power*, Vol. 13, No. 5, 1997, pp. 635–642.

[15]Rogers, R. C., and Schexnayder, C. J., Jr., "Chemical Kinetic Analysis of Hydrogen-Air Ignition and Reaction Times," NASA TP 1856, July 1981.

[16]Mitani, T., "Ignition Problems in Scramjet Testing," *Combustion and Flame*, Vol. 101, No. 3, 1995, pp. 347–359.

[17]Radhakrishnan, K., and Bittker, D. A., "LSENS, A General Chemical Kinetics and Sensitivity Analysis Code for Homogeneous Gas-Phase Reactions," NASA RP 1329 and 1330, March 1994.